Effect of a Directionally Porous Wing Tip on Tip Vortex

M. Aldheeb[1], W. Asrar[1†], A. Omar[2], A. Altaf[3] and E. Sulaeman[1]

[1] Department of Mechanical Engineering, International Islamic University Malaysia (IIUM), Kuala Lumpur, 63100, Malaysia
[2] School of Aerospace and Automotive Engineering, International University of Rabat, Recade Rabat-Sale 11100 Sala El Jedida, Morocco
[3] New York Institute of Technology, Abu Dhabi Campus -UAE

†Corresponding Author Email: waqar@iium.edu.my

ABSTRACT

This paper presents an experimental study of the effect of a directionally porous wing tip on the tip vortex using particle image velocimetry (PIV) on a half wing model with NACA 653218 as its airfoil section. Four different configurations of the directionally porous wing tip are tested. The vortex generated by the wing tips are examined at four different measuring planes downstream perpendicular to the flow axis. The flow field over the porous wing tip surface along the streamwise direction is obtained as well to understand the effects of the porosity on the flow which in the end affects the vortex downstream. Furthermore, the aerodynamic performance of all different configurations is compared to study their effects on the aerodynamic coefficients of the wing. The results show a high reduction in vorticity, up to 90%; tangential velocity reduction up to 67% and a significant reduction in vortex circulation in the near-far field. Effect on the lift to drag ratio is up to 20 %.

NOMENCLATURE

α	angle of attack	CM	wing moment coefficient
AR	wing aspect ratio	Re_c	Reynolds number based on chord length
c	chord	xac	aerodynamic center
$C1, C2$	configuration 1, 2, ..	P	porosity
CL	wing lift coefficient	PIV	Particle Image Velocimetry
CD	wing drag coefficient	x/c	measuring location from wing trailing edge
CD, i	induced drag coefficient		

1. INTRODUCTION

The idea of a porous wing tip is borrowed from birds. The tip of a bird's wing consists of several separated feathers with controllable gap distance and gap orientation between these feathers which depend on the flight conditions. Bird wings are complex in structure and design and have not been thoroughly studied Aldheeb *et al.* (2016). Several researchers have studied the bird wing tips either by looking at the bird's wing itself or by mimicking (modeling) them. Numerous studies have been done on wing tips to reduce the induced drag and reduce vortex strength generated by wing tips, downstream. A grid at the wing tip was introduced by La Roche and Palffy (1996) to reduce the induced drag. The grid is an add-on device with a small chord attached to the wing tip. They concluded that it has a maximum effect on rectangular wings where the reduction in total drag is up to 40%, and in elliptic wings, the reduction is only about 3%. A similar wing tip with a small modification, mimicking a bird's wing tip was studied by Smith *et al.* (2001) in which the effect of multiple wing tips on drag reduction using a force balance in a wind tunnel was studied. The results showed no significant effect on aerodynamic performance (mainly reduction in drag). However, it shows diffusion in tip vortex based on flow visualization. Different wing tip devices were studied by Céron-Muñoz *et al.* (2013) to evaluate the

reduction in induced drag; multi-wing tip devices produced the maximum drag reduction. CFD simulation was performed on three different winglet designs by Narayan and John (2016) to study their effect on reducing the induced drag. The mutli-tip-4 winglet produced the highest lift while the muti-tip-3 winglet produced higher lift to drag ratio for low aspect ratio wing and, the base wing produced high lift to drag ratio for high aspect ratio wing

A balsa feather-like tip was introduced by Tucker (1993), who also studied a Clark-Y tip and a tip with mounted Hawk feathers. The Clark-Y tip produced the highest lift to drag ratio (L/D) followed by the Hawk feather tip. Balsa feather-like tip resulted in a smaller L/D compared to others. However, Hawk feather tip produced higher L/D than others at an angle of attack $\alpha = 12^\circ$ and more.

A CFD study was carried out Sachs and Moelyadi (2006) to study the effect of a slotted tip, which contributed to a significant aerodynamic moment resulting in yaw stability.

A spiroid winglet was used and an increase in the lift and its slope by 9% and improvement in L/D by about 7% werw noticed by Guerrero *et al.* (2012). It also increased the parasite drag due to increase in surface area.

The effect of live bird tips on induced drag was studied by Tucker (1995). In this study, Hawk birds were used in the experiments with complete wing tips and their behavior was compared to a wing with clipped tip feathers. The induced drag factor of the wing with complete wing tips was 0.56 and increased to 1.1 when feathers were clipped. However, the results do not verify whether the reduction of induced drag is due to tip slots, the flexibility of tip feather or both.

The present study introduces a new porous tip and studies the effect of the directional porosity of this tip on the aerodynamic performance and the flow field. Particle Image Velocimetry (PIV) is used to study the flow field and tip vortex. A wind tunnel force balance is also used to measure the lift and drag.

2.1 Wake Vortex Alleviation

The wake vortex generated by wing tips are the strong roll-up of the flow which is slow in dissipation rate. Wing add-on devices increased the rate of vortex strength reduction and decreased the vortex roll-up intensity in the near and far field, Rossow (1991)

Add-on devices have been introduced in many studies to alleviate the effect of the wake vortex created by the wing tip. PIV was used to examine the wake vortex in the near-wake field of a scaled half-model aircraft with differential spoiler setting (DSS) (Altaf *et al.,* 2015; Elsayed *et al.,* 2010). The study showed a significant change in the wing loading affected by the spoiler and flap wake vortices. The same spoiler (DSS) was studied experimentally using PIV for a high-lift configuration wing, Elsayed *et al.* (2011). The DSS for the same model was studied numerically by Ludin *et al.* (2013) and

similar results were found as in the experiments which had a reduction of approximately 44 % in cross flow velocity upon deploying the spoiler. Add-on devices such as spoilers on wing tip (Corsiglia *et al.* (1971), splines downstream on the tip (Patterson (1975); delta-type plates on the outboard flap (Breitsamter (2011), half-delta wing (Lee and Pereira, (2013), and reverse-delta wing (Altaf *et al.,* 2015; Coustols *et al.,* 2006) were used to alleviate the wake vortex. The investigation of wake vortex generation by using supplementary vortex generators to modify the tip vortex has been studied experimentally by Heyes and Smith (2005) using PIV. By merging the vortices from wingtip and vortex generator, the results show a significant redistribution of wake circulation.

The effect of wing tip blowing on wake vortex has been studied by Margaris and Gursul (2010) using PIV. The blowing from near pressure surface results in vortex diffusion, while the jet produces opposite results if positioned near the suction surface. The study of the rounded and squared tip was studied Giuni and Green (2013) using PIV and found out that the squared tip produced multiple vortices due to the two sharp edges. PIV experiments on three different wing tip configurations namely square-cut, simple fairing, and Whitcomb's full winglet were carried out by Sohn and Chang (2012) at different angles of attack. The results of Whitcomb's full winglet shows a reduction in wing tip vortex and increase in lift to drag ratio compared to other configurations. The wake vortex coming from Whitcomb's winglet is more diffused and weaker. The effect of free stream turbulence on wake vortex and aerodynamic performance was studied by Ahmadi-Baloutaki *et al.* (2015) using hot-wire measurements on a NACA 0015 wing section. The results show that free stream tends to increase the diffusion of the vortex. The synthetic jet actuation seems to affect the wake vortex of wing tip as studied experimentally by Dghim *et al.* (2016) using hotwire. The results show a stretching of vortex shape into an elliptical one at higher momentum coefficients and low frequency near the trailing edge. At further downstream, the vortex regains its normal shape, but with a reduction in its strength.

2. EXPERIMENTAL SETUP

The experiments were performed in the International Islamic University Malaysia (IIUM) Low-Speed closed-circuit wind tunnel. It has a maximum speed of 50 m/s and turbulence intensity less than 0.11%. The test section has dimensions of 6 m × 2.3 m × 1.5 m. The half model normal force has a measurement range of ±2000 N and has an uncertainty of 0.04 %. The axial force has a measurement range of ±700 N and has an uncertainty of 0.05%. The pitching moment has a measurement range of ±250 N.m and has an uncertainty of 0.04%. The measurement uncertainty in lift and drag coefficients is 2% and the uncertainty in moment coefficient is 2.5% The measurements have a confidence level of 95% and based on this the uncertainty in velocity is ± 0.19 m/s

The PIV tests were carried out at a wind speed of 12

m/s ($Re_c = 1.87 \times 10^5$). This low speed allows the PIV camera to capture the moving particles better than at higher speeds.

The PIV test setup consists of the wind tunnel, model wing, SAFEX fog generator, a Flow Sense M2 8-bit camera with Nikon 60 mm lens and a New Wave Solo laser (Fig. 1 and Fig. 2). The fog generator used in this experiment uses SAFEX fog fluid which generates 1 micron sized seeding particles. A dual frame laser is used with a time of 40 microseconds between pulses. For each test, seven bursts are used and at each burst nine recordings are made which results in a total of 1110 images. These images are averaged to produce one image consisting of real vectors. The high number of recordings per test is preferred (instead of several recordings at different times), which produces a more comprehensive and representative vector image of the tip vortex. Also, substituting vectors during PIV data analysis is avoided.

Three types of experiments have been performed for each model to study the effect of directional porosity. The first set of experiments use PIV to determine the vortices downstream of the flow to investigate the effect of different directional porosity models on tip vorticity. The tip vortex experiments are carried out at four different measuring planes in the flow direction (x-direction) as shown in (Fig. 3). The vortex results will be presented for a wing angle of attack α of 15º and results at α = 5º and 10º will be tabulated. The second set of experiments are PIV measurements on the flow field over the upper wing tip surface for an angle of attack α = 15º to study the effect of directional porosity. The third experiment is to determine the effect of each type of wing tip on the aerodynamic loads using a six-component force balance. The lift, drag and moment coefficients are presented for wing tip models with different directional porosities.
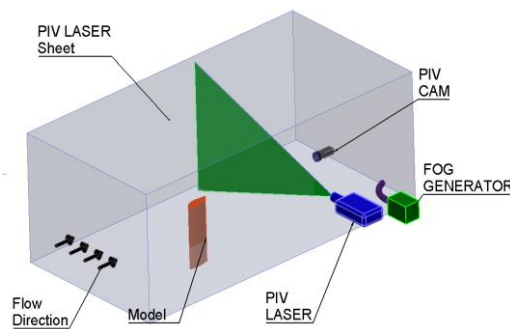
finish and filled edges, the wingtip design is a cut-off wingtip based on Raymer (1999). The base model wingtip is shown in Fig. 4. All other configuration results will be compared to this base configuration to investigate the effect of directional porosity on vorticity and tangential velocity (TV) downstream of the wing tip at each measuring location for a wing angles of attack of 5º, 10º and 15°.
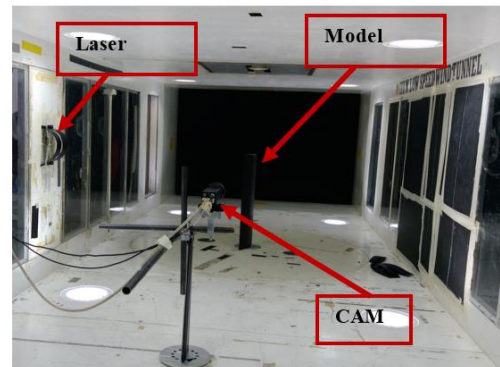

Fig. 2. PIV setup inside IIUM Low Speed Wind Tunnel.

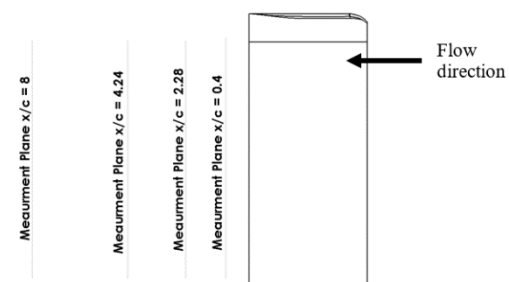**Fig. 3. Measuring locations of tip vortex (measured from wing trailing edge).**

Fig. 1. Schematic of PIV setup in the wind tunnel.

2.1 Configuration1 (Base Model C1)

Four different wingtip models (configurations, C) have been selected for the experiments. All models are straight wings made of solid aluminum, with NACA 653218 as their airfoil section. The first configuration (C1) is the base model (clean, straight, half-span wing model) (Fig. 4). C1 is the base model which is a wing with no modification to its tip, its surface is non-porous, and it has a smooth surface
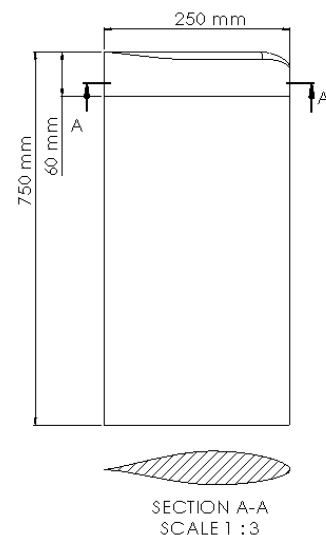

Fig. 4. Base wing configuration NACA 653218 section (model 1).

2.1 Configuration 2 (C2)

The second configuration (C2) (Fig. 5) is a wing with

porous tip, the porosity on the tip is inclined at 45° toward the free stream flow direction. This inclined porosity allows the flow through the porous surface to be more aligned with the flow direction especially at a high angle of attack (α), as shown in Fig. 5.
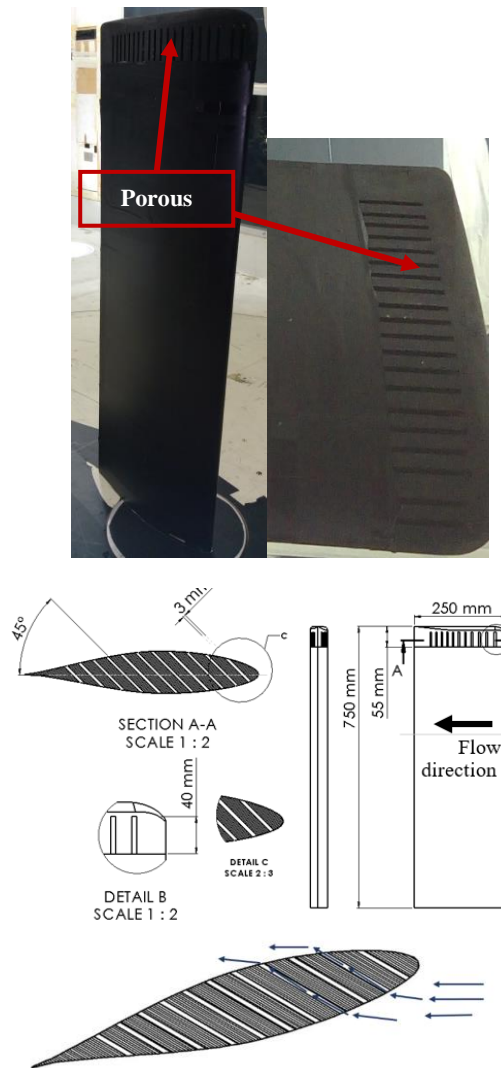
**Fig. 5. Wing model dimensions with tip porosity (C 2).**

2.1 Configuration 3 (C3)

The third configuration C3 is similar to the second configuration but with different porosity inclination. Model 3 (Fig. 6) has a porosity inclination of 90° (perpendicular to the flow stream at α = 0º). Wingtips of configurations C2 and C3 are made of wood, and the porosity is represented by 3 mm openings with a spacing of about 10 mm between each opening as shown in (Fig. 5 and Fig. 6). The openings are not throughout the wing tip but begin at 20 mm from the wing tip (spanwise) and have a length of 40 mm (spanwise).

2.1 Configuration4 (C4)

The fourth configuration (C4) is a high porosity tip made of an aluminum honeycomb structure, and the porosity direction is perpendicular to the flow

direction similar to C3. Fig. 7 shows the sketch of the honeycomb tip and the dimensions where the honeycomb has a porosity of about 93%. The honeycomb has a cell size of 5 mm and cell wall thickness of 0.08 mm.
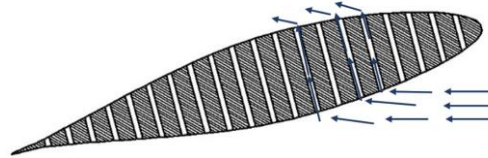
Fig. 6. C3 wingtip cross-section with porosity inclination 90º, at α = 15º.
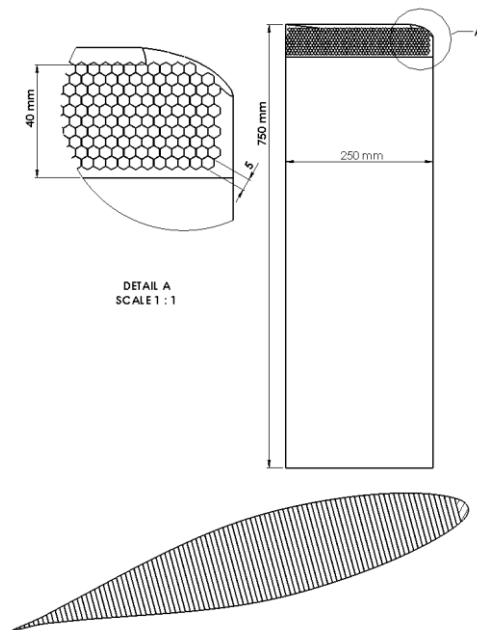
Fig. 7. Wing with honeycomb tip (C4).

3. VORTEX FLOW

As mentioned earlier, the vorticity is measured at four different planes in the downstream direction which are (x/c) = 0.4, 2.28, 4.24, and 8, from the wing trailing edge. The vorticity contours and tangential velocities are analyzed using Dantec Flow Map software. Note that, the measuring location (x/c), free stream velocity (V∞), the angle of attack (α) and the configuration (C1, 2, 3 or 4) are mentioned on all figures. The figures below represent the results for all models at two measuring planes and for one angle of attack (15º). To reduce the large number of figures, the remaining results are shown in Table 1 to 4.

Fig. 8 shows the vorticity contours for all models together at the four-measuring planes where it shows the general reduction in vorticity at an angle of attack α = 15º. The base model (C1) has maximum vorticity values of -3035/s, -2078/s, -2026/s, and -1618/s at measuring planes (x/c) = 0.4, 2.28, 4.24, and 8, respectively. The negative sign shows the vorticity rotational direction only, the positive sign is counterclockwise. The vorticity contours and

tangential velocity vector maps for measuring planes (x/c) = 2.28 and 8 are shown in Fig. 9. The figures show that the vorticity and the tangential velocity are evenly distributed around the vortex core. This indicates that the vorticity is generated and developed by the wingtip without any disturbance to the flow.
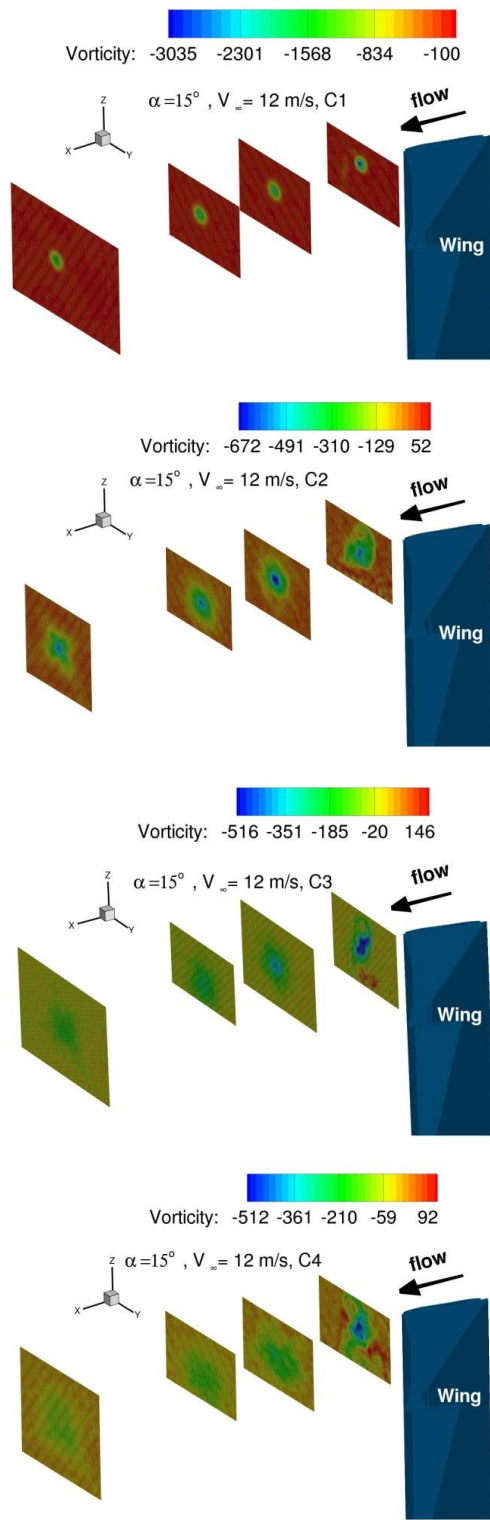

Fig. 8. Vorticity contours for (C 1, C2, C3 and C4) at (x/c) = 0.4, 2.28, 4.24 and 8.

Moving to the second configuration C2 which is the model with a porous wingtip with a directional porosity at 45° to the chord. The maximum vorticity contours are -566/s, -675/s, -553/s, and -557/s at measuring planes (x/c) = 0.4, 2.28, 4.24, and 8, respectively. These values result in a vorticity reduction of 81%, 68%, 72%, and 62%, at the same measuring planes (x/c), respectively. Fig. 10 shows the vorticity contours and tangential velocity vectors. Some distortion of the tangential velocity around the vortex core resulting in an uneven distribution of the tangential velocity is observed. The flow passing though the directionally porous wing tip affects the flow stream on the upper surface of the wing tip resulting in a reduction in vorticity in the near wake field. Further details about the tangential velocity and flow field over the upper surface of the wing tip will be explained in the following sections.

Increasing the inclination of the porosity to 90° in C3 to be perpendicular to the chord line results in further disturbance of the flow as shown in Fig. 11 where the vorticity contours appear to be vanishing especially at (x/c) = 8. The maximum values of vorticities at (x/c) = 0.4, 2.28, 4.24, and 8 are -516/s, -375/s, -259/s, and -163, respectively. These values show a reduction of 83%, 82%, 87%, and 90% compared to the configuration C1 at the same measuring planes, respectively.

Configuration 4 (C4) has a high porosity geometry as mentioned earlier. The vorticity and tangential velocity contours in Fig. 12 are shown at (x/c) = 2.28 and 8, the vorticity behavior is similar to the vorticity for configuration C3 especially at (x/c) = 8. It shows that higher porosity causes a higher effect on vorticity where the values of vorticity are -512/s, -276/s -177/s, and -135/s resulting in a reduction of 83%, 87%, 91%, and 92 % at (x/c) = 0.4, 2.28, 4.24, and 8, respectively.
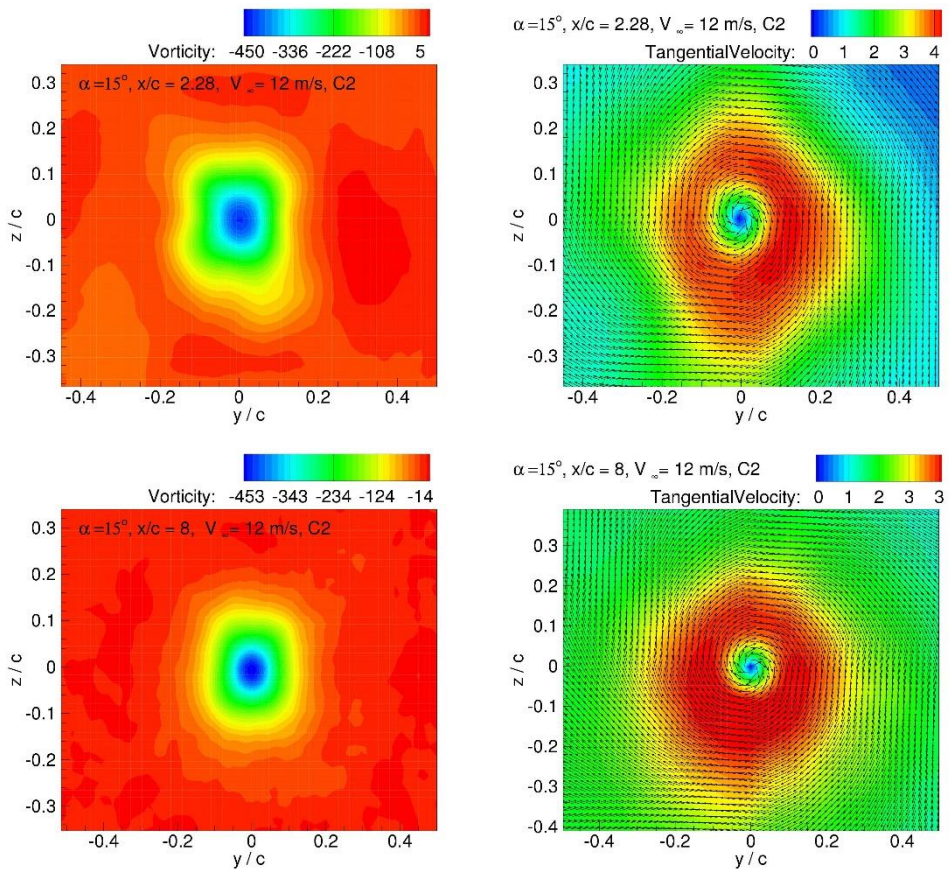
4. TANGENTIAL VELOCITY DISTRIBUTION AND CIRCULATION

2.1 Tangential Velocity Distribution

The vorticity contour shapes at all locations downstream of the wing tip for the base model (C1) are uniformly distributed, and the tangential velocity around the vortex is almost constant. On the other hand, the modified models (C2 – C4) have a non-uniform distribution of the tangential velocity due to the effect of the directionally porous wing tips. Thus, the average tangential velocity is computed to be able to calculate the circulation. The tangential velocity is normalized as $V\theta / V\infty$ where $V\theta$ is the tangential velocity, and $V\infty$ is the free stream flow velocity. The radius is also normalized as r / c where c is the wing chord.
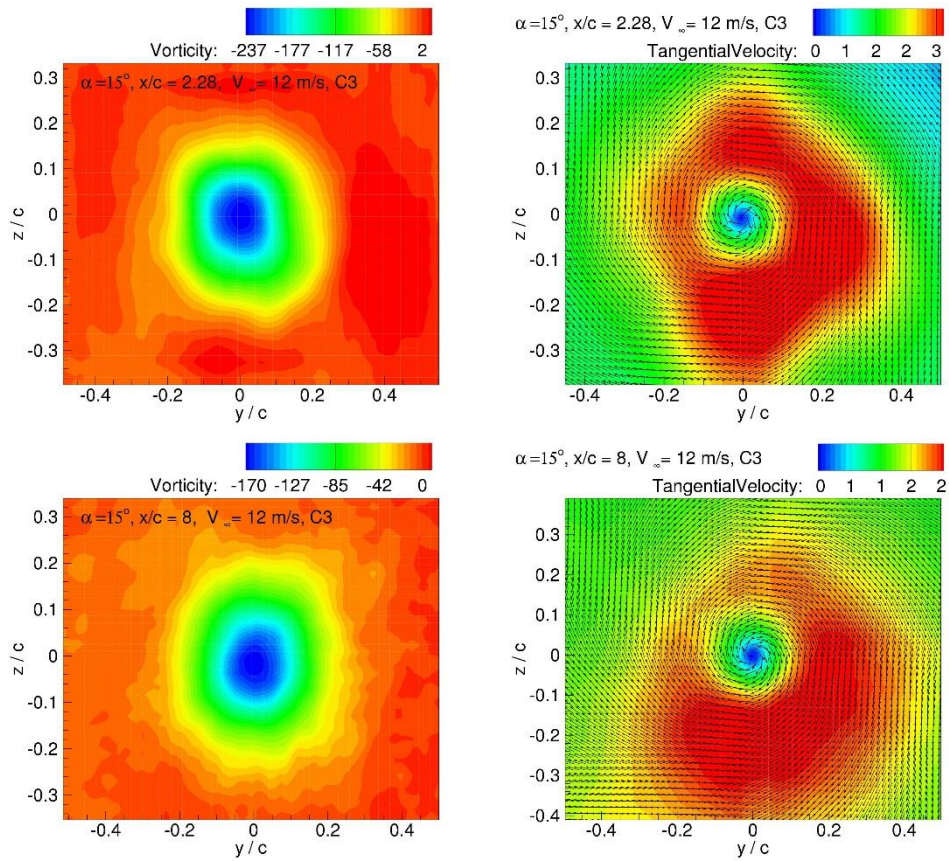
The tangential velocity distributions are presented in Fig. 13. The reduction in average tangential velocities at (x/c) = 0.4 compared to C1 are 55%, 57% and 60% for C2, C3, and C4, respectively. At this measuring location, almost all models have a similar reduction in percentage. The directional porosity of the wing tip affects the flow behavior and destroys the uniformity of the vorticity contours. The
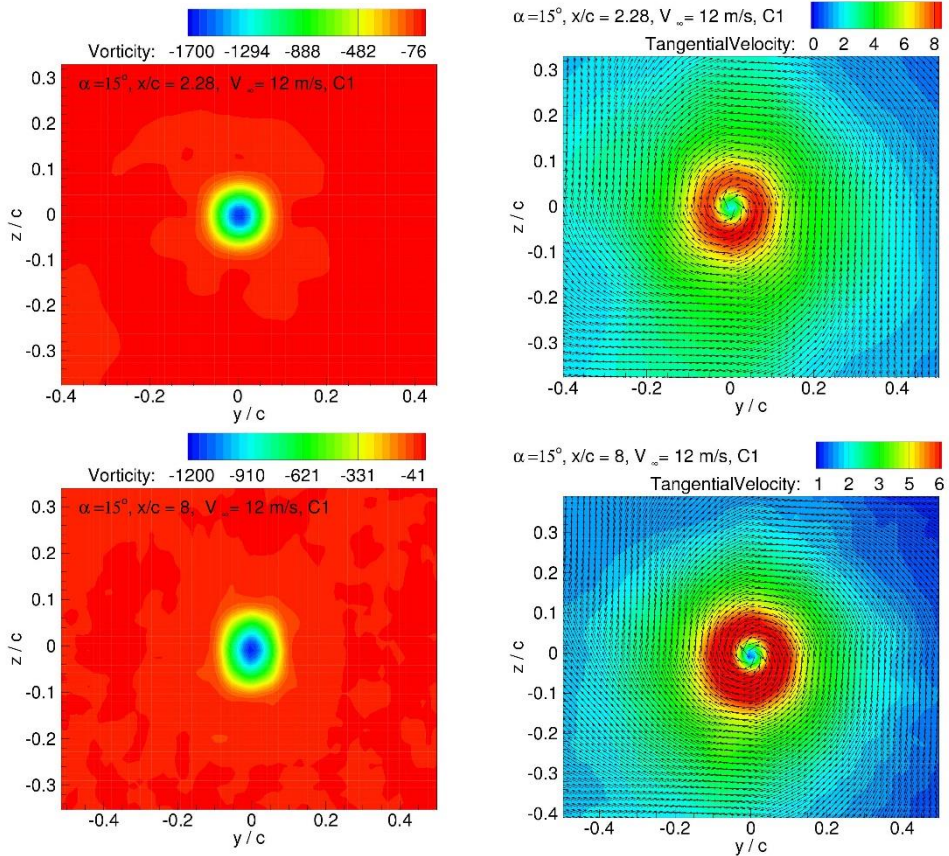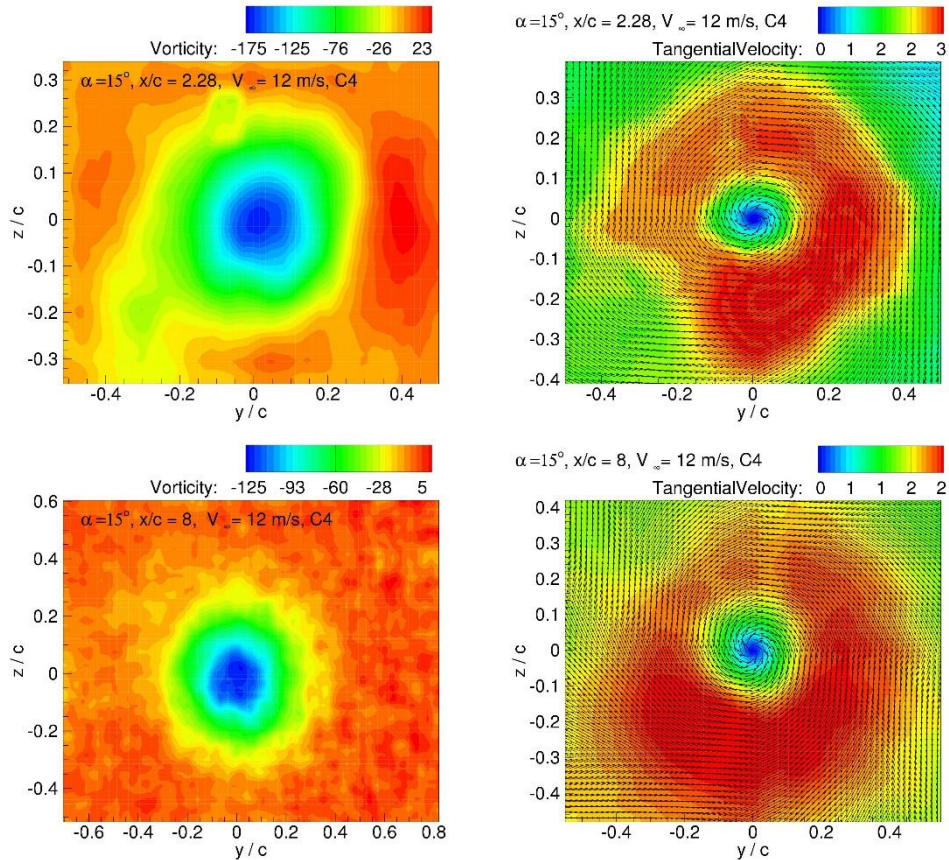
Fig. 9. Vorticity and Tangential Velocity of C1 at (x/c) =2.28 and 8.

Fig. 10. Vorticity and Tangential Velocity of C2 at (x/c) =2.28 and 8.

Fig. 11. Vorticity and Tangential Velocity of C3 at (x/c) =2.28 and 8.

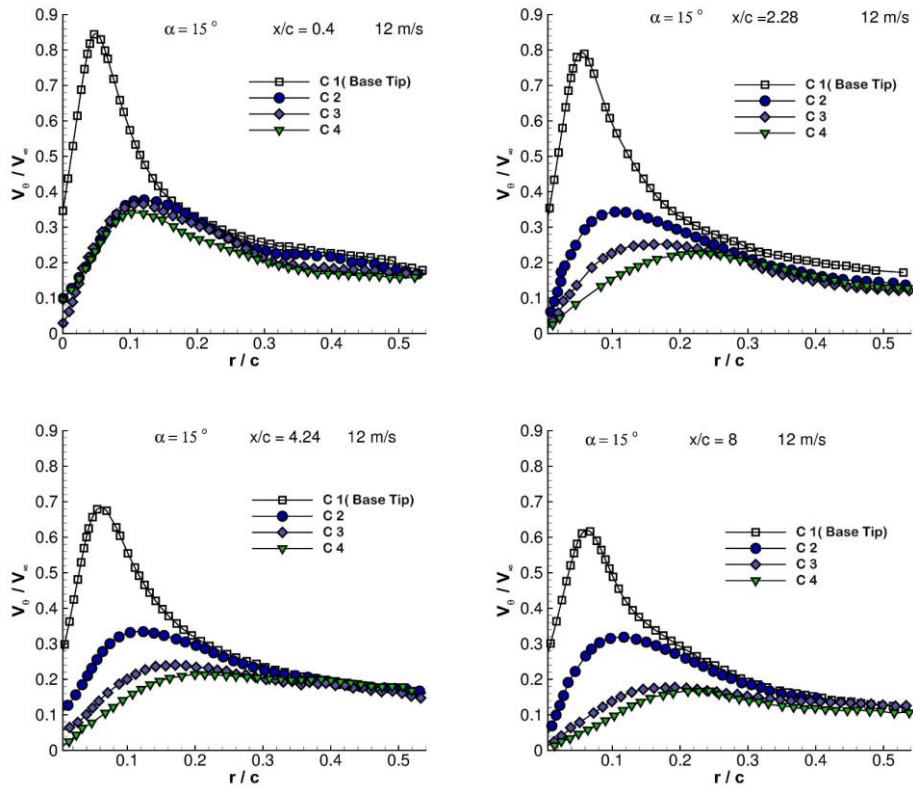**Fig. 12. Vorticity and Tangential Velocity of C4 at (x/c) =2.28 and 8.**

Fig. 13. Tangential velocity distribution, x/c = 0.4, 2.28 4.24, and 8.

Table 1 Changes in vorticity, tangential velocity, and radius compared to base mode (C1) in percentages for all configurations at (x/c) = 0.4

α	Vorticity			Tangential velocity			Radius		
	C 2	C 3	C 4	C 2	C 3	C 4	C 2	C 3	C 4
5°	-15%	-39%	-79%	-13%	-31%	-60%	10%	17%	144%
10°	-65%	-80%	-80%	-54%	-54%	-58%	126%	136%	93%
15°	-81%	-83%	-83%	-56%	-57%	-60%	137%	128%	122%
20°	-67%	-72%	-79%	-41%	-51%	-56%	89%	116%	114%

effect increases as the porosity inclination becomes increasingly perpendicular to the chord line. The similarity in tangential velocity reduction in all models is due to the measurement location which is close to the trailing edge where (x/c) = 0.4. The differences in the tangential velocity and its distribution due to directional porosity are more pronounced further downstream.

The modified models (C2 - C4) affect the radius of the vortex and increase it by 137%, 129% and 122% in C2, C3, and C4, respectively.

Similarly, at (x/c) = 2.28, the average tangential velocity (Fig. 13) has a reduction of 57%, 68% and 71% in models C2, C3, and C4, respectively. At this measuring location, the tangential velocity reduction varies from one model to another. Models C3 and C4 have the highest effect on the velocity distribution. The vortex radius increases by 99%, 201% and 326% for the models C2, C3, and C4, respectively. As the radius increases significantly in C3 and C4, the

reduction in tangential velocity is high. At (x/c) = 4.24, the average tangential velocity for models C2, C3, and C4 (Fig. 13) has a reduction of 51%, 65% and 69%, respectively and these reduction percentage are similar to the reduction at (x/c) = 2.28.

At the last location of measurement (x/c) = 8, the reduction in average tangential velocity are 49%, 71% and 73% in C2, C3, and C4, respectively, as shown in Fig. 13. This farthest plane has the maximum reduction in average velocity for C3 and C4. The effect of model C2 is less than 50% at any measuring location which indicates its limited impact compared to configurations C3 and C4 in which their effect on velocity reduction reaches up to 71% and 73%, respectively.

The radius of the vortex increases by 90% (C2), 212% (C3) and 287% (C4) and the same conclusion that higher reduction in average tangential velocity results in an increase in vortex radius is reached. This indicates that the vortex is diffusing faster as

Table 2 Changes in vorticity, tangential velocity, and radius compared to base mode (C1) in percentages for all configurations at (x/c) = 2.28

α	Vorticity			Tangential velocity			Radius		
	C 2	C 3	C 4	C 2	C 3	C 4	C 2	C 3	C 4
5º	-65%	-83%	-91%	-41%	-62%	-69%	24%	138%	436%
10º	-85%	-89%	-93%	-69%	-64%	-67%	248%	181%	376%
15º	-68%	-82%	-87%	-57%	-68%	-72%	98%	201%	326%
20º	-45%	-69%	-81%	-27%	-39%	-50%	68%	93%	185%
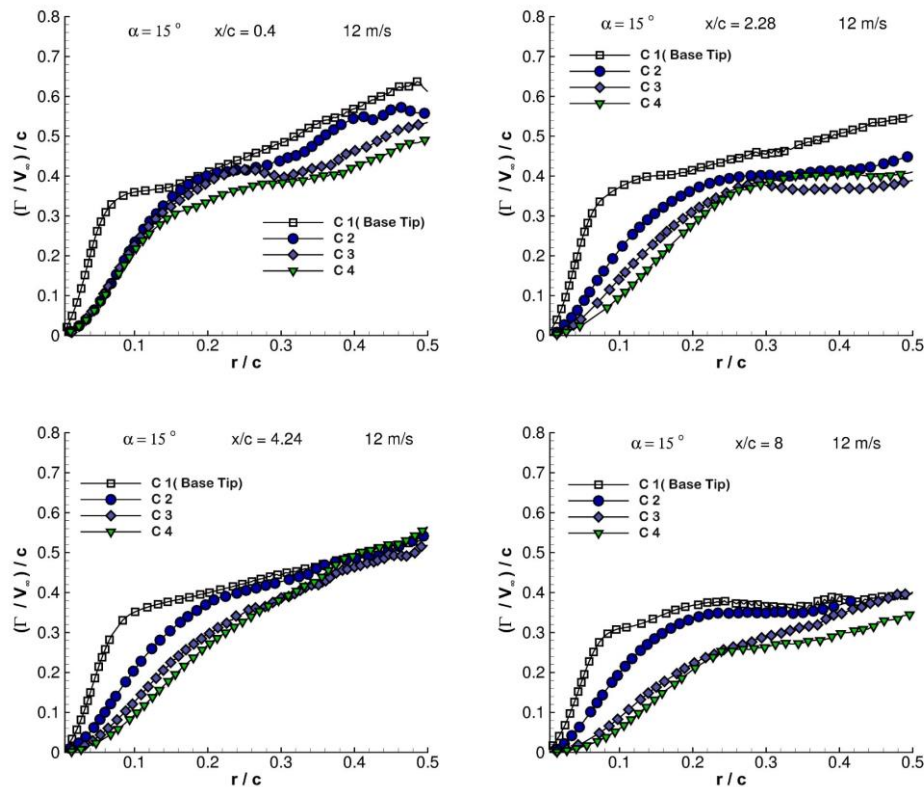
Fig. 14. Circulation at x/c = 0.4, 2.28 4.24, and 8.

compared to the base model.

The changes in vorticity, tangential velocity, and radius for all directional porosities are shown in Table 1 to Table 4 for all models at all measuring planes for wing angles of attack of α = 5º, 10º, 15º and 20º in percentage. At α = 5º and (x/c) = 0.4, (Table1) C4 has the highest effect of vorticity and tangential velocity reduction almost twice the effect of C3 and three times the effect of C2. For the same measuring plane, at α = 10º, the effect of C3 is similar to the effect of C4. At (x/c) = 2.28, C2, C3, and C4 have a significant effect on vorticity and tangential velocity reduction at all α as shown in Table2. It can be seen that at α = 10º, the effect of the porous wing tip is higher than other angles of attack. At the other measuring planes (x/c) = 4.24 and 8, the effect of each porous wingtip at different angles of attack is similar. More details are shown in Table 3 and Table 4.

2.1 Circulation

As the tangential velocity distribution is known, the circulation can be calculated. Circulation is defined as $\Gamma = \int_0^r \int_0^{2\pi} \zeta dA$ (Anderson, 2016; Dobrev *et al.,* 2008), this definition yields the following equation

$$\Gamma = 2\pi r V_\theta \qquad (1)$$

where Γ is the circulation, r is the radius (r = 0 at vortex core), and V_θ is the averaged tangential velocity at the radius (r).

The effect of a directionally porous tip is noticeable from the first measuring plane (x/c) = 0.4 as shown in Fig. 14. It can be seen at r/c = 0.01 – 0.15, that the reduction in circulation is high especially at low values of radius and at r/c =0.1 the reduction can reach up to 24% and 25% for C3 and C4, respectively. The effect reduces as the radius increases where at r/c = 0.2, the reduction is about 6% and 18% for C3 and C4, respectively. The effect of C2 on circulation is very small compared to C3 and C4 especially at a measuring plane near the trailing edge where (x/c) =0.4. As the vortex travels further downstream, the effect of the directionally

Table 3 Changes in vorticity, tangential velocity, and radius compared to base mode (C1) in percentages for all configurations at (x/c) = 4.24

	Vorticity			Tangential velocity			Radius		
α	C 2	C 3	C 4	C 2	C 3	C 4	C 2	C 3	C 4
5°	-70%	-89%	-94%	-70%	-69%	-74%	164%	248%	420%
10°	-88%	-90%	-91%	-68%	-68%	-70%	355%	305%	347%
15°	-72%	-87%	-91%	-52%	-65%	-69%	88%	145%	234%
20°	-49%	-66%	-79%	-30%	-44%	-52%	42%	103%	164%

Table 4 Changes in vorticity, tangential velocity, and radius compared to base mode (C1) in percentages for all configurations at (x/c) = 8

	Vorticity			Tangential velocity			Radius		
α	C 2	C 3	C 4	C 2	C 3	C 4	C 2	C 3	C 4
5°	-87%	-89%	-93%	-58%	-58%	-49%	884%	740%	785%
10°	-86%	-86%	-91%	-62%	-64%	-99%	595%	679%	-96%
15°	-66%	-90%	-92%	-49%	-72%	-73%	90%	211%	287%
20°	-31%	-53%	-51%	-7%	-23%	-39%	15%	40%	314%

porous tip increases especially in models C3 and C4 as shown in Fig. 14. At (x/c) = 2.28 the circulation reduced by 36%, 57% and 72% at r/c = 0.1 for C2, C3 and C4. As the radius increases to r/c = 0.2, the effect reduces to 12%, 25% and 32% for C2, C3 and C4, respectively. It can be noticed that C2 has a smaller impact on circulation reduction compared to C3 and C4. At (x/c) = 4.24, the reduction increases to 42%, 64% and 73% for C2, C3 and C4, respectively at r/c = 0.1. At r/c = 0.2, the reduction is 6%, 26% and 33% for C2, C3 and C4, respectively. At the farthest plane downstream, (x/c) =8, the effect of a directionally porous tip is most significant and is shown in Fig. 14. The model C4 has the maximum reduction in the circulation values followed by C3. At r/c = 0.1, the reduction in circulation is 44%, 75%, 83% for C2, C3, and C4 respectively, while at r/c = 0.2, the reduction is 9% 39% and 43% for C2, C3 and C4. The high reduction in circulation is due to the high reduction in tangential velocities especially at low values of the radius. The general behavior of circulation for the base model shows that it increases rapidly at low values of radius and then starts to increase slowly as the tangential velocity reaches nearly free stream values. Introduction of the directionally porous tips changes the behavior of circulation and it increases slowly as the radius increases. It can be seen from the figures below that all directionally porous wing tips show consistently lower circulation than the base model. The configurations C3 and C4 have the highest effect on vorticity, tangential velocity, vortex radius and circulation due to the directional porosity being perpendicular to the free stream direction.

5. FLOW OVER THE WINGTIP SURFACE

This section presents the effect of directional porosity on the flow field over the wingtip surface.

PIV measurements were made on the upper surface

of each tip for the flow in the streamwise direction as shown in Fig. 15.

The PIV results of the flow field over the wing tip models are shown in Fig. 16 to Fig. 19. Wing tip C1 (base model) shows smooth flow at α = 15° as shown in Fig. 16. In the model C2, it can be seen from Fig. 17 that there is a small disturbance of the flow near the boundary layer of the upper surface of the wing tip. This disturbance is due to the directional porosity at 45° in the tip. The strongest effect of directional porosity on the flow field occurs in models C3 and C4 as shown in Fig. 18 and Fig. 19, respectively, as the directional porosity in these two cases, is perpendicular to the chord line/free stream direction. This disturbance of the flow disturbs the vortex during its formation. It results in a huge reduction in vortex strength values as explained earlier in the vortex section where the reduction can reach up to 87% and 90 % in configurations C3 and C4, respectively.

The effect of the porosity increases the size of the low-velocity region due to the velocity passing through the porous structure and interacting with the stream flow over the top surface of the wingtip. In C2 where the porosity has an inclination of 45°, the low-velocity layer near the upper surface can reach up to 0.06c at the middle point of the wing chordwise, and near the trailing edge, the layer can reach up to 0.06c as shown in Fig. 17. This region increases dramatically in C3 and C4 where the porosity is perpendicular to the chord line causing a higher disturbance of the stream flow on the upper wingtip surface, the low-velocity region/layer in C3 can reach up to 0.13c at the midpoint of the tip chordwise and 0.15c at the trailing edge as shown in Fig. 18. As the porosity increases the region/layer of low-velocity increases as in C4 where the wingtip has high porosity region resulting in a higher amount of fluid flow passing from the lower to the upper surface through the porous structure. The layer
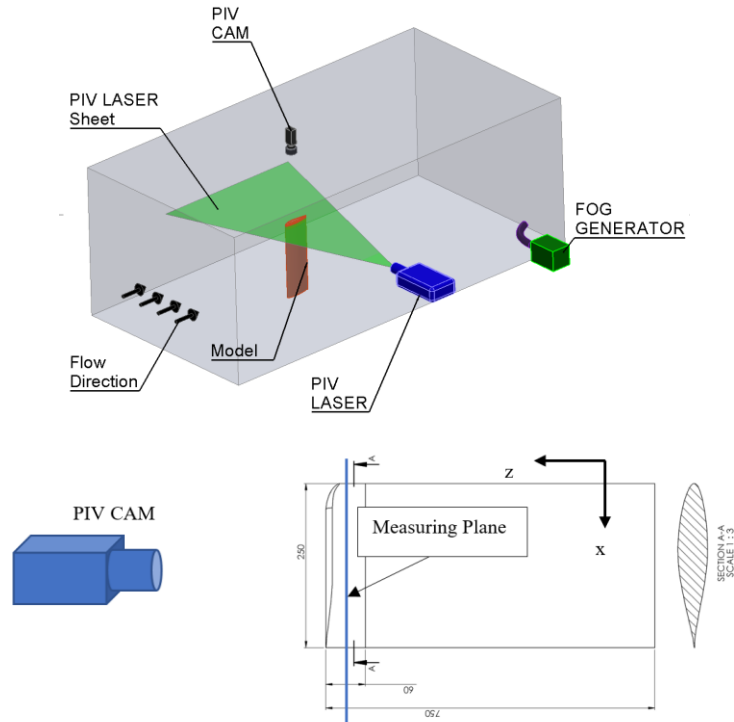
Fig. 15. Setup sketch for PIV experiment of flow field over porous tip and measuring plane (mm).
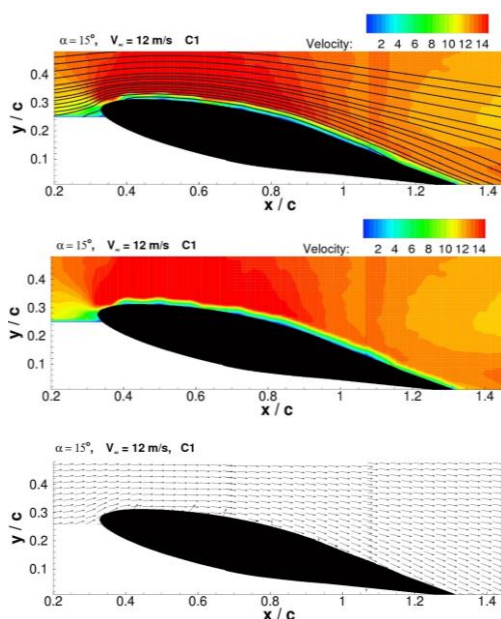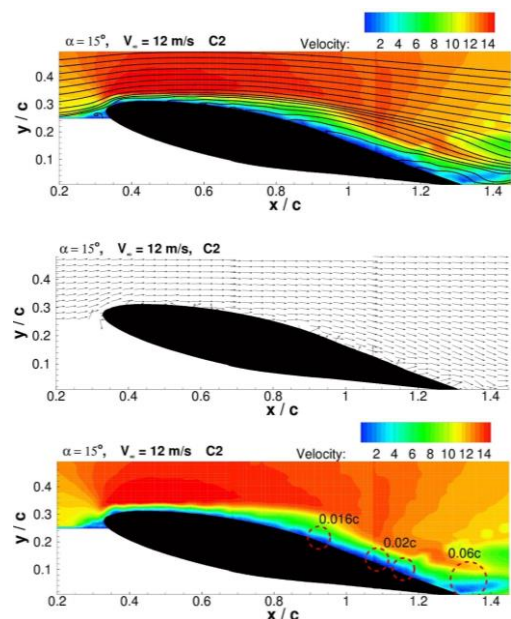

Fig. 16. Flow over C1 (base) tip at α = 15°.

Fig. 17. Flow over tip, C2 at α = 15°.

region of low velocity over the wingtip surface can reach up to 0.168c – 0.21c, as shown in Fig. 19.

It can be concluded that disturbing the vortex formation during its early stages results in a high reduction of the vortex strength values downstream.

6. AERODYNAMIC PERFORMANCE

In this section, the effect of directionally porous tips

on the coefficients of lift, drag and moments are presented. The lift to drag ratio (L/D) is the most critical parameter in aerodynamic performance, the change in lift and drag are also discussed here. In the previous sections, the effect of the directional porosity on vortex and downstream flow is analyzed, and both C3 and C4 produce the best results regarding vortex strength reduction. However, the combination of earlier results together with aerodynamic performance will help to decide the
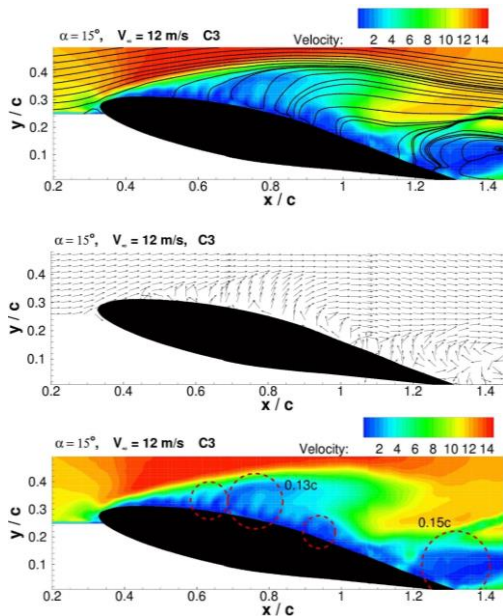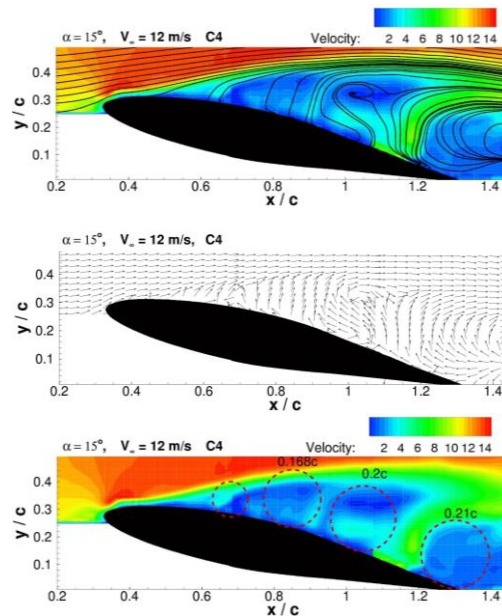
Fig. 18. Flow over tip, C3 at α = 15º.

Fig. 19. Flow over tip, C4 at α = 15º.

Table 5 Changes in lift and drag coefficients for all configurations compared to other wake alleviation devices

Authors	Device	Lift Reduction	Drag Increment
Porous wingtips	C2	4%	11%
	C3	5.5%	14%
	C4	4.5%	18%
Altaf *et al.* (2015)	Add-on Reverse delta wing	4.9%	11.3%
Breitsamter (2011)	Double delta spoiler	2.9%	unavailable
Rosso (1978)	Fins	No lift penalty	10%
Croom and Holbrook (1979)	Fins	13.3%	28.6%
Oslash *et al.* (2001)	Wing control surfaces and fins	7.0%	unavailable

best configuration for vortex alleviation.

The effect of wing tips with directional porosity on lift coefficient especially at low angles of attack is small. It can be seen from Fig. 20, the lift coefficients do not change for the range of α = [-10° - +10°]. At higher angles of attack, there is a small decrease in the lift for the porous tips (C2 - C4) compared to the base model. Likewise, the drag coefficients of C2 and C3 are close to the base model, and the increase in drag coefficients is noticeable in C4 (Fig. 21). Looking at the L/D ratio in Fig. 23, there is a decrease in the lift to drag ratio (L/D) especially at angles of [5° -10°] for models C 2, C3 and C4. Model C4 has a larger effect at higher angles of attack α= [5°-15°].

The maximum reduction in L/D occurs at α = 6º which is about 20%. Model C3 has smaller drag coefficients than C4 and thus has better L/D performance. Increase in drag especially in C4 is perhaps due to the increased surface area for the flow to go through due to the high porosity of the honeycomb structure.
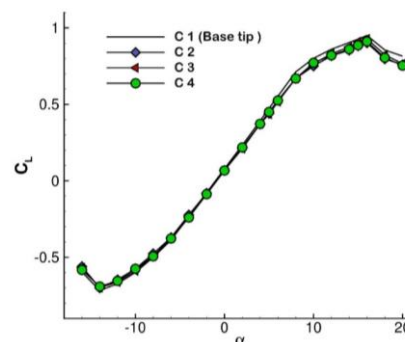

Fig. 20. Lift coefficients CL vs angle of attack α for all Configurations.

The effect on moment coefficients (Fig. 22) is minimal, and all models behave similarly. Thus, porous tips have a negligible effect on aerodynamic moment coefficients. As shown Table 5, C4 has the highest increase in drag coefficients which can reach up to 21%. C3 has a relatively high increase in drag compared to other models, which can reach up to

14% at. C2 has less drag and has the best aerodynamic performance. Combining the results of flow vortex and aerodynamic performance, models C3 and C4 have the best overall performance regarding reduction in vortex strength downstream of the wing. The drawback of model C4 is that it has high drag increment, however, if the model is optimized regarding the structure and surface modification it could be the best model as it has the highest reduction in vorticity, tangential velocity, and circulation. As the vortex experiment is carried out at α=5º, 10º and 15º, considering the aerodynamic performance at these angles, model C3 seems to be the best model as it has less increase in drag compared to C4 and also it has a large effect on circulation reduction, close to C4. The lift and drag penalties of these models are compared to previous vortex alleviation devices aerodynamic penalties as shown in Table 5.
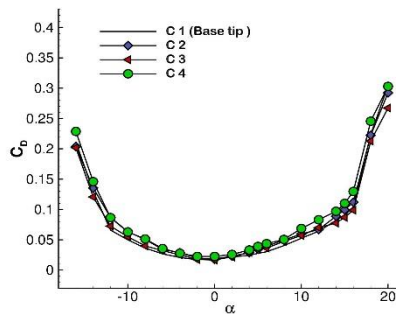

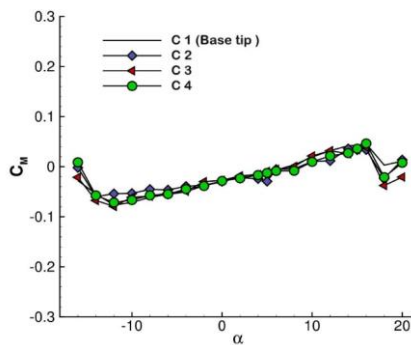**Fig. 21. Drag coefficients CD vs angle of attack α for all Configurations.**

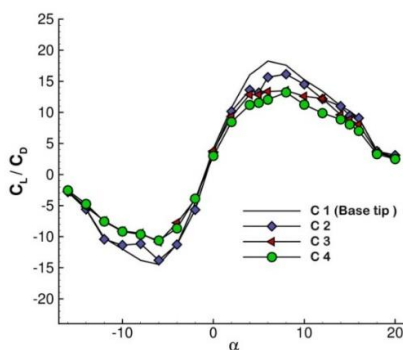**Fig. 22. Moment coefficients CM vs angle of attack α for all Configurations.**
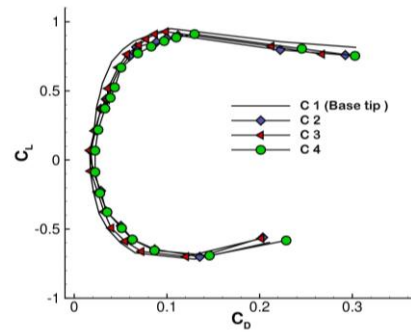

Fig. 23. Lift to drag ratio vs α.

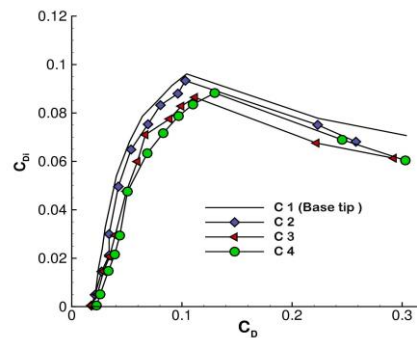**Fig. 24. Drag polar (CD vs CL) for all Configurations.**

Fig. 25. Induced vs total drag.

2.1   Induced Drag

Induced drag s calculated using the following equation

$$C_{D,i} = \frac{C_L^2}{\pi e AR} \tag{2}$$

where $C_{D,i}$ is the induced drag coefficient, C_L is the lift coefficient, e is the efficiency factor, and AR is the aspect ratio.

Fig. 25 shows a slight reduction in induced drag when using models C3 and C4 compared to the base model. Thus, it can be concluded that the slight increment in total drag for models C3 and C4 is perhaps due to the viscous effects caused by the high flow separation on the upper surface of the wing tip as explained earlier and shown in Fig. 18 and Fig. 19.

7.   CONCLUSION

This research focuses on the effect of porous wing tips with directional porosity on the flow field over the wingtip surface, its impact on the vorticity

formation and strength downstream, and the aerodynamic performance of the wing. PIV is used to capture the flow field behavior over the wingtip surface and to measure the vorticity downstream at four measuring planes. Four different models were compared at α =5º, 10º, and 15º; the results show a significant impact on vorticity, tangential velocity, and circulation reduction by introducing highly porous wing tips with porosity in a certain direction. Models C3 and C4 produce the highest reduction in

vortex strength among all models. The aerodynamic performance shows a small effect on lift due to porous tips and higher effect on drag especially in model C4 which is perhaps due to the increased surface area due to the high porosity of the honeycomb structure. Combining all effects of vorticity, tangential velocity, circulation and aerodynamic performance it can be concluded that model C3 (porosity perpendicular to the chord line/free stream) has the best performance which has the highest reduction in vorticity, tangential velocity, and circulation, close to C4. Furthermore, C3 has less drag increase due to the tip porosity compared to C4. Even though there is a decrease in the L/D ratio,

directional porosity during the landing phase can perhaps be used for wake vortex alleviation. Further detailed studies are required to determine the optimum direction and magnitude of porosity for maximum lift to drag ratio and optimum aerodynamic performance for any specific wing.

REFERENCES

Ahmadi-Baloutaki, M., R. Carriveau and D. S. -K. Ting (2015). An experimental study on the interaction between free-stream turbulence and a wing-tip vortex in the near-field. *Aerospace Science and Technology* 43, 395-405

Aldheeb, M. A., W. Asrar, E. Sulaeman, A. A. Omar (2016) A review on aerodynamics of non-flapping bird wings. *Journal of Aerospace Technology and Management* 8, 7-17

Altaf, A., T. B. Thong, A. A. Omar, W. Asrar (2015) Influence of a Reverse Delta-Type Add-On Device on Wake Vortex Alleviation. AIAA Journal, 54(2), 625-636.

Anderson, J. D. (2016). *Fundamentals of Aerodynamics*. McGraw-Hill Education,

Breitsamter, C. (2011) Wake vortex characteristics of transport aircraft. *Progress in Aerospace Sciences* 47, 89-134

Céron-Muñoz, H. D., R. Cosin, R. Coimbra, L. Correa and F. Catalano (2013). Experimental investigation of wing-tip devices on the reduction of induced drag. *Journal of Aircraft,* 50(2), 441-449.

Corsiglia, V. R., R. A. Jacobsen and N. Chigier (1971). An experimental investigation of trailing vortices behind a wing with a vortex dissipator. In: *Aircraft wake turbulence and its detection.* Springer, 229-242

Coustols, E., L. Jacquin and G. Schrauf (2006). Status of wake vortex alleviation in the framework of European collaboration: validation using tests and CFD results. *European conference on computational fluid dynamics, ECCOMAS CFD*

Croom, D. R. and G. T. Holbrook (1979). Low-speed wind-tunnel investigation of wing fins as trailing-vortex-alleviation devices on a transport airplane model. *NASA Langley Research Center; Hampton*, VA, United States.

Dghim, M., M. Ferchichi, R. E. Perez, M. BenChiekh (2016). Near wake development of a wing tip vortex under the effect of synthetic jet actuation. *Aerospace Science and Technology* 54, 88-107

Dobrev, I., B. Maalouf, N. Troldborg and F. Massouh (2008). Investigation of the wind turbine vortex structure. In: *14th international symposium on applications of laser techniques to fluid mechanics*, Lisbon, Portugal, 07-10

Elsayed, O. A., W. Asrar, A. A. Omar and K. Kwon (2010) Influence of differential spoiler settings on the wake vortex characterization and alleviation. *Journal of Aircraft* 47, 1728

Elsayed, O. A., A. A. Omar, W. Asrar and K. Kwon (2011). Effect of differential spoiler settings (DSS) on the wake vortices of a wing at high-lift-configuration (HLC). *Aerospace Science and Technology* 15, 555-566

Giuni, M. and R. B. Green (2013). Vortex formation on squared and rounded tip. *Aerospace science and technology* 29, 191-199

Guerrero, J. E., D. Maestro and A. Bottaro (2012). Biomimetic spiroid winglets for lift and drag control. *Comptes Rendus Mecanique* 340, 67-80

Heyes, A. L. and D. A. Smith (2005). Modification of a wing tip vortex by vortex generators. *Aerospace science and Technology* 9, 469-475

La Roche, U. and Palffy, S. (1996) Wing-grid, a novel device for reduction of induced drag on wings. In: *ICAS PROCEEDINGS,*. 2303-2309

Lee, T. and J. Pereira (2013). Modification of static-wing tip vortex via a slender half-delta wing. *Journal of Fluids and Structures* 43, 1-14

Ludin, H. B., A. A. Omar and W. Asrar (2013). Numerical Study of the Effect of Spoiler Configuration on Wake Vortex Alleviation. *Journal of Aerospace Engineering* 28, 04014077

Margaris, P. and I. Gursul (2010). Vortex topology of wing tip blowing. *Aerospace science and technology* 14, 143-160

Narayan, G. and B. John (2016). Effect of winglets induced tip vortex structure on the performance of subsonic wings. *Aerospace Science and Technology* 58, 328-340

Oslash, E., zger, I. Schell and D. Jacob (2001). On the structure and attenuation of an aircraft wake. Journal of Aircraft, 38(5), 878-887.

Patterson, J. C. (1975). Vortex attenuation obtained in the Langley vortex research facility. *Journal of Aircraft* 12, 745-749

Raymer, D. P. (1999). Aircraft design: a conceptual approach, American Institute of Aeronautics and Astronautics *Inc, Reston, VA* 21

Rosso, V. J. (1978). Effect of wing fins on lift-generated wakes. *Journal of aircraft* 15, 160-167

Rossow, V. J. (1991). Prospects for alleviation of

hazard posed by lift-generated wakes. In: *Proceedings of the Aircraft Wake Vortices Conference*, 29-31

Sachs, G. and A. A. Moelyadi (2006). Effect of slotted wing tips on yawing moment characteristics. *Journal of theoretical biology* 239, 93-100

Smith, M., N. Komerath, R. Ames, O. Wong and J. Pearson (2001). Performance analysis of a wing with multiple winglets. *In 19th AIAA Applied Aerodynamics Conference* (p. 2407).

Sohn, M. H. and J. W. Chang (2012). Visualization

and PIV study of wing-tip vortices for three different tip configurations. *Aerospace Science and Technology* 16, 40-46

Tucker, V. A. (1993). Gliding birds: reduction of induced drag by wing tip slots between the primary feathers. *The Journal of Experimental Biology* 180, 285-310

Tucker, V. A. (1995). Drag reduction by wing tip slots in a gliding Harris' hawk, Parabuteo unicinctus. *The Journal of experimental biology* 198, 775-781